Article

pubs.acs.org/Biomac

Characterization of Mesoscale Coiled-Coil Peptide–Porphyrin Complexes

Brian J. Pepe-Mooney, Bashkim Kokona, and Robert Fairman*

Department of Biology, Haverford College, 370 Lancaster Avenue, Haverford, Pennsylvania 19041, United States

Supporting Information

ABSTRACT: Photoelectronically conductive self-assembling peptide–porphyrin assemblies have great potential in their use as biomaterials, owing largely to their environmentally responsive properties. We have successfully designed a coiled-coil peptide that can self-assemble to form mesoscale filaments and serve as a scaffold for porphyrin interaction. In our earlier work, peptide–porphyrin-based biomaterials were formed at neutral pH, but the structures were irregular at the nano- to microscale size range, as judged by atomic force microscopy. We identified a pH in which mesoscale fibrils were formed, taking advantage of the types of porphyrin interactions that are present in well-characterized J-aggregates. We used UV–visible spectroscopy, circular dichroism spectropolarimetry, fluorescence spectroscopy, and atomic force microscopy to characterize these self-assembling biomaterials. We propose a new assembly paradigm that arises from a set of unique porphyrin–porphyrin and porphyrin–peptide interactions whose structure may be readily modulated by changes in pH or peptide concentration.

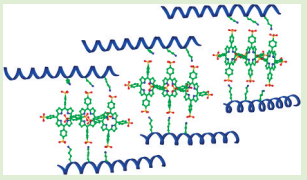

INTRODUCTION

Advances in the design and synthesis of protein- and peptide-based biomaterials have led to their applications in tissue engineering,[1] biomineralization,[2] and photoelectronics,[3−5] for example. The advantages imparted by incorporation of polypeptide-based biological reagents into biomaterials include responsiveness to environmental conditions and reversible behavior.[4,6−8]

We have been interested for some time in using peptides and porphyrins to create photoelectronically active biomaterials in which the peptide acts as a coiled-coil scaffold for binding an anionic porphyrin and modulating its activity.[9−11] Coiled coils have been an attractive protein structural motif for biomaterial development because their folding and oligomeric assembly are so precisely understood, and several recent reviews have been written on this topic.[12−14] Likewise, porphyrins have been studied for some time because of their promise in photoelectronic applications. Particular attention has focused on *meso*-tetrakis(4-sulfonatophenyl)porphine ($TPPS_4$) because of its ability to self-assemble into structures referred to as H-aggregates and J-aggregates.[15,16] More effort has been directed toward studying the biomaterial properties of J-aggregates because this mesoscale structure is better understood.[17−30] $TPPS_4$ J-aggregates readily assemble at low pH (<2.0) when two of the four sulfonates have been neutralized (Figure 1). The large-scale structure of J-aggregates arises from arrays of slipped face-to-face stacking interactions between individual units;[20] these interactions result in the formation of nanorods and nanoribbons in the mesoscale size range based on imaging studies.[17,19,21,28−30] J-Aggregates have a clearly defined spectroscopic signature (Table 1) making them easy to identify, with a strongly red-shifted Soret band at 490 nm (J-band) and a second band at 705 nm (Q_x-band).[31,32] H-Aggregates typically occur at high porphyrin concentrations. While H-aggregates also involve some type of face-to-face interaction, the details of these interactions remain obscure, and their resultant mesoscale morphologies are not uniform. The spectroscopic signature of H-aggregates is more heterogeneous but often results in blue-shifting of the Soret band.[33] Many laboratories have taken advantage of these self-assembling properties of $TPPS_4$, and other ionic porphyrins, to create photoelectronic biomaterials often in association with a wide variety of other biomacromolecules, including carbohydrates,[34,35] nucleic acids,[36,37] lipids,[38−40] and polypeptides.[41−62]

Most of the focus in creating hybrid porphyrin-based materials has been on using peptides and proteins, because self-assembly, responsiveness, and fine-tuning photoelectronic

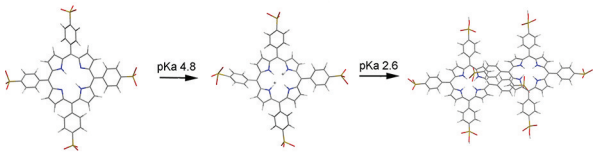

Figure 1. Chemical structures of $TPPS_4$ at different protonation states and dimer structure of the J-aggregate conformation.

Table 1. UV-Visible Absorbances of the Different pH Forms of $TPPS_4$

structure	Soret band (nm)	Q bands (nm)
free base ($H_2TPPS_4^{4-}$)	413	516, 553, 579, 633
diacid ($H_4^{2+}TPPS_4^{4-}$)	434	594, 645
J-aggregate ($H_4^{2+}TPPS_4^{2-}H_2$)	490	705

Received: June 20, 2011
Revised: October 25, 2011
Published: October 27, 2011

activity is a desirable feature in such biomaterials. General protein binding studies have been carried out to explore effects on porphyrin photoelectronic activity,[41,42,49,56,58] but a more precise structural understanding for binding has been explored through peptide−porphyrin studies involving either noncovalent interactions[43,44,48,52,54,55,57,59−63] or covalent peptide−porphyrin linkages.[45−47,53,64] As suggested above, our interest has been to study the binding of an anionic porphyrin, $TPPS_4$, to a positively charged coiled-coil peptide model system to create structurally well-defined biomaterials. Several research laboratories have taken advantage of this anionic porphyrin in peptide binding studies,[52,57,59,61,62] most notably in recent work from Kuciauskas and Caputo.[50,51]

We demonstrated the successful development of a photoelectronically active biomaterial using $TPPS_4$ in association with our designed coiled-coil peptide scaffold in our recently published work.[9] We found that our designed peptide, Cp3K, interacted with the negative sulfonate groups on the $TPPS_4$ molecule through three appropriately positioned positively charged lysine groups such that, upon binding, the porphyrin induced a helical structure in the peptide (see model in Figure 6A). This amphipathic peptide was designed to polymerize upon helix formation through helix−helix interactions involving interactions between hydrophobic amino acids spaced according to the rules governing coiled-coil assembly.[11] Although we were successful in the above-mentioned efforts, the lengths and heights of the polymers were not homogeneous, as imaged by atomic force microscopy (AFM). These amorphous structures caused us to re-evaluate the conditions under which these porphyrin−peptide complexes were assembled. We thought that we could take advantage of J-type interactions in $TPPS_4$ to create more uniform fibrils, as suggested by Kuciauskas and Caputo.[50,51] Formation of J-aggregates of $TPPS_4$ require extremely low pH conditions in which the center nitrogens are fully protonated (pK_a of 4.8) and two of the four sulfonates are neutralized (pK_a of 2.6).[35] Thus, above a pH of 4.8, the porphyrin exists in its free base form, whereas between a pH of 2.6 and 4.8, the porphyrin is in its diacid form. At a pH below 2.6, the first two sulfonate groups of $TPPS_4$ are protonated causing the porphyrins to form J-aggregates (Figure 1).

We hypothesized that the addition of the same basic peptide that we used at neutral pH[9] could act to neutralize two sulfonates at slightly acidic conditions (in which the ring nitrogens are fully protonated) to promote J-aggregation, while at the same time providing the polymerizing scaffold that had been engineered into this peptide. We test this hypothesis here by probing the spectroscopic and morphological properties of the resultant polymer.

EXPERIMENTAL SECTION

Peptide Synthesis and Purification. The synthesis and purification of Cp3K was done as described previously.[9] Briefly, the synthesis of Cp3K was carried out on an Applied Biosystems (Foster City, CA) 433A peptide synthesizer using standard FMOC chemistry and using PAL resin (Advanced ChemTech, Louisville, KY). The peptide was purified using a Varian ProStar (Varian, Inc., Palo Alto, CA) system equipped with a Varian Dynamax semipreparative C18 column. The peptide identity was confirmed using MALDI-TOF mass spectrometry.

Solution Preparation. Lyophilized peptide was dissolved in Milli-Q-filtered water to make stock solutions and was split into 50 μL aliquots and frozen at −80 °C for storage purposes. Peptide stock solution concentrations (1−2 mM) were determined by using a modified ninhydrin procedure.[65] Porphyrin stock solutions (<1 mM) were prepared by dissolving *meso*-tetrakis(4-sulfonatophenyl)porphine ($TPPS_4$; Frontier Scientific Inc.) in 6 mM NaOH. The concentration was determined using $\varepsilon_{414} = 5.33 \times 10^5\ M^{-1}\ cm^{-1}$.[31]

UV−Visible Spectroscopy. UV−visible data were collected using a 1 mm cuvette on a Lambda 25 UV/vis spectrophotometer (Perkin-Elmer Instruments, Waltham, MA). Wavelength scans were collected from 300 to 800 nm at room temperature using a wavelength step size of 1.0 nm. Samples were prepared in 20 mM formic acid buffer at pH 3.5 unless otherwise specified. The pH profile experiment was conducted using 20 μM $TPPS_4$ and 20 μM Cp3K in 10 mM each of the sodium salts of phosphate, citrate, and borate. The kinetic data were fit to the following kinetic function to extract quantitative information about the lag and the time constants:

$$y = \frac{A_1 - A_2}{1 + e^{(x - x_0)/dx}} + A_2$$

in which A_1 and A_2 are the starting and ending absorbance signals, dx is the time constant for the transition, and x_0 represents the center of the transition along the x-axis, thus, defining the lag in the kinetics.

Circular Dichroism Spectropolarimetry. CD data were collected on an Aviv Associates (Lakewood, NJ) model 202-01 CD spectropolarimeter. Wavelength scans were performed at 25 °C in the range of 198 to 250 nm for the peptide bands, and 350 to 550 nm for the porphyrin bands, using a wavelength step size of 1.0 nm or less. Data points represent 3 s of averaging time. All samples were measured in 20 mM formic acid, pH 3.5, unless stated otherwise.

Fluorescence Spectroscopy. Fluorescence spectra were collected using a Fluorolog-2 spectrofluorometer (Spex Industries, Inc., Edison, NJ) under the control of SPEX DM3000F software. Data were collected using a 1 mm cuvette containing 6.67 μM Cp3K and 20 μM $TPPS_4$ in 20 mM formic acid, pH 3.5. Scans were performed at room temperature using an excitation wavelength of 453 nm. Emissions spectra were collected in the range of 550−800 nm using increments of 1 nm and an integration time of one second.

Atomic Force Microscopy. AFM data were collected in tapping mode using a Bioscope atomic force microscope (Digital Instruments, Santa Barbara, CA). Samples were prepared in 20 mM formic acid, pH 3.5 at appropriate peptide−porphyrin ratios and incubation times required for complex formation. Samples were deposited on a freshly cleaved mica (SPI Supplies, West Chester, PA) surface for 10 min at room temperature in a constant humidity chamber. After incubation, excess liquid was drained, and the mica surfaces were gently dried under nitrogen.

Molecular Modeling. The $TPPS_4$ structures shown in Figure 1 were generated and energy minimized using the MM2 force field, as implemented in ChemBioDraw Ultra v. 12.0.3 (CambridgeSoft, Cambridge, MA). The starting molecular model for the structure in Figure 6A, containing the 1:1 Cp3K/$TPPS_4$ oligomer, was taken from our published model.[9] In brief, molecular mechanics were run in INSIGHTII 2000 (Biosym Technologies, San Diego) using a combination of steepest descents and conjugate gradients to optimize the docking of the helix pairing interactions.[11] In a separate exercise, the $TPPS_4$ structure was docked manually to optimize ionic interactions between three of the four sulfonates and appropriately spaced lysines on the peptide, and the Bump_Check function in InsightII 2000 was used to eliminate van der Waals clashes.[10] These structures were used to create the Cp3K-$TPPS_4$ oligomer described above.[9] Two polymers were then manually docked in a staggered conformation, using Discovery Studio 2.1 (Accelrys, San Diego) to suggest the potential for H-type interactions between two of the porphyrins.

The second model, in Figure 6B, containing the 2:3 Cp3K/$TPPS_4$ building block, was built using the same peptide scaffold as described in our previous work.[9] The $TPPS_4$ structures were docked onto this model using Discovery Studio 2.1 (Accelrys, San Diego), maintaining the appropriate distance for ionic interactions between the lysine ε-amino groups on the peptide and the sulfonates on the $TPPS_4$ and avoiding steric clashing between adjacent porphyrins using the Bump_Check function.

RESULTS AND DISCUSSION

Our overarching goal was to identify solution conditions that would result in improving the quality of the fibrillar structures formed in our Cp3K–$TPPS_4$ assemblies. We decided to take advantage of the interactions between $TPPS_4$ molecules that result in J-aggregation with the thought that it would improve the fibril persistence length and the homogeneity of the lateral fibril dimensions. At the same time, we wanted to maintain important interactions between the porphyrin and the peptide in order to modulate photoelectronic activity. The ability of $TPPS_4$ to form J-aggregates depends on acidic pH conditions, while the folding of the peptide is largely pH-independent because its interactions are driven by the hydrophobic effect. As a consequence, we took advantage of this difference in pH sensitivity to explore alternative conditions and to promote favorable mesoscale structural properties. In the process of identifying appropriate pH conditions for these experiments, we encountered two additional variables that came into play, including kinetic effects and the effects of different peptide–porphyrin stoichiometries.

These three variables, pH, kinetics, and stoichiometry, result in a complex interplay that required careful analysis to deconvolute their influences on the assemblies, as we describe in this work. For the sake of clarity, we first present the experiments to understand the role of pH on self-assembly. While we will show that kinetic and stoichiometric variables play a role in modulating the pH response, the major finding from our pH work is to offer evidence for J-aggregation to justify the conclusion that a new structure has been discovered.

Starting initially with a 1:1 ratio of Cp3K and $TPPS_4$, we explored a pH range of 2–9 to look for spectral characteristics that might suggest a peptide-modulated J-aggregation assembly process. As a control, we monitored the spectroscopic signature of $TPPS_4$ by itself as a function of pH. The results for $TPPS_4$ alone (Figure S1A) confirm the known absorbance characteristics (Table 1) of the different protonated structures (as illustrated in Figure 1). Importantly, the J-aggregate signature for $TPPS_4$ becomes prominent only at pH values well below 3.0, as the first set of two sulfonates become protonated, whereas, for the Cp3K–$TPPS_4$ complex, the J-aggregate signature appears at significantly higher pH, where the diacid form of the porphyrin dominates (Figure 2). The peptide thus appears to replace the neutralization function of the protons on the two sulfonates necessary to foster J-aggregate growth.[66] Similar electrostatic effects have been observed in the presence of NaCl, confirming this interpretation.[15] While kinetic and stoichiometric effects (see below) play a role in defining the magnitude of the absorbance of this 490 nm band, this band is always present to some degree under the relevant conditions explored in this work.

We chose a pH of 3.5 for further experimentation because it optimized the yield of J-aggregate in the presence of the peptide. At this pH, $TPPS_4$ is not prone to aggregate on its own, and the diacid form (represented by the 434 nm band) of the porphyrin is the dominant species available for peptide binding. The extent of J-aggregation in the presence of the peptide and at pH 3.5 is shown in Figure 3A (note spectrum for the latest time point; see also Figure S2 for clarity). The bands at 416/424 nm in these spectra arise from peptide–porphyrin interactions that do not involve J-aggregation; we had noted this signature for peptide–porphyrin interactions at pH 7.8 as well (Figure S2) in previously published work.[9] The slow

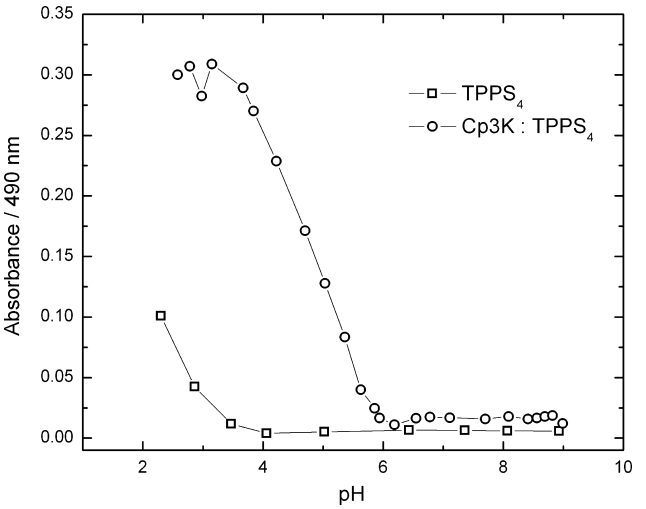

Figure 2. pH dependence of 490 nm band in the absence or presence of Cp3K. The porphyrin and peptide concentrations were 20 μM each, prepared in 10 mM each of the sodium salts of phosphate, citrate, and borate, and measured at 25 °C.

increase in the magnitude of the 490 nm band over time will be described in more detail below.

Having established that Cp3K can bind $TPPS_4$ in the J-aggregate form at low pH, we then asked if peptide binding depends upon secondary structure. Cp3K by itself exhibits only partial helical structure under acidic conditions, as seen by CD, containing less than 20% helix content (Figure 3B) and is largely monomeric (as determined by sedimentation equilibrium analysis; data not shown). When an equimolar quantity of $TPPS_4$ is added, two minima in the peptide CD spectrum appear, one at 208 nm and a second at 225 nm. This new spectrum suggests that the Cp3K peptide acquires >80% helical structure upon binding $TPPS_4$. However, a quantitative treatment of helix content should be treated with caution because there is an apparent red shift of the helical band that normally lies at 222 nm; such a red shift, coupled with an effect on the relative intensities of the 208 and 222 nm bands, has been interpreted previously as due to a light scattering effect associated with an aggregating system.[9,47,67] The helical form of the peptide is acquired rapidly upon mixing with $TPPS_4$ and is stable over time, suggesting that no significant precipitation is occurring over the time frame of the experiments described herein. The rapid acquisition of helix content suggests that any and all complexes formed must require a helical conformation for binding. Nevertheless, we do note a subtle decrease in the 208 nm band over time, which mirrors the kinetic effect observed in the UV–visible spectroscopy data (Figure 3A). This decrease could represent a slight increase in the degree of soluble aggregation. As shown previously, $TPPS_4$ also acquires CD bands in the Soret region upon peptide binding, indicative of an induced chiral environment;[9] however, the intensity of this band emerged more slowly, as seen in the inset to Figure 3B, and is consistent in time constant to that observed for the loss of the 208 nm signal. We also note the bisignate band centered around 490 nm in the CD spectrum, again consistent with J-aggregate formation; this induced CD band has been observed by others as well.[50] From the initial pH profile data and subsequent CD analysis, it was clear to us that the Cp3K–$TPPS_4$ complex contains porphyrin J-aggregates with peptide

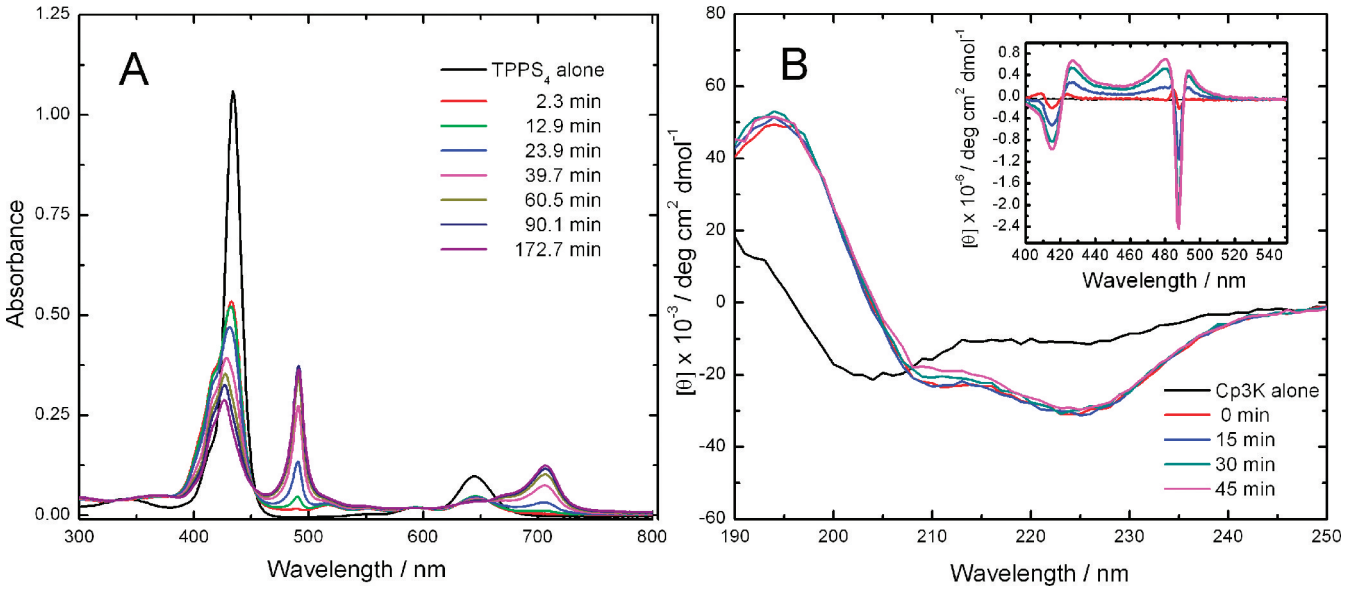

Figure 3. Dependence on time for UV–visible and CD spectra. (A) Absorbance spectra of $TPPS_4$ alone and in the presence of Cp3K as a function of time. The porphyrin and peptide concentrations were 20 μM each, prepared in 20 mM formic acid, pH 3.5, and measured at 25 °C. (B) CD spectra of Cp3K alone and in the presence of $TPPS_4$ as a function of time. Inset: porphyrin CD as a function of time (black line: $TPPS_4$ alone). The porphyrin and peptide concentrations were 20 μM each, prepared in 20 mM formic acid, and measured at 25 °C.

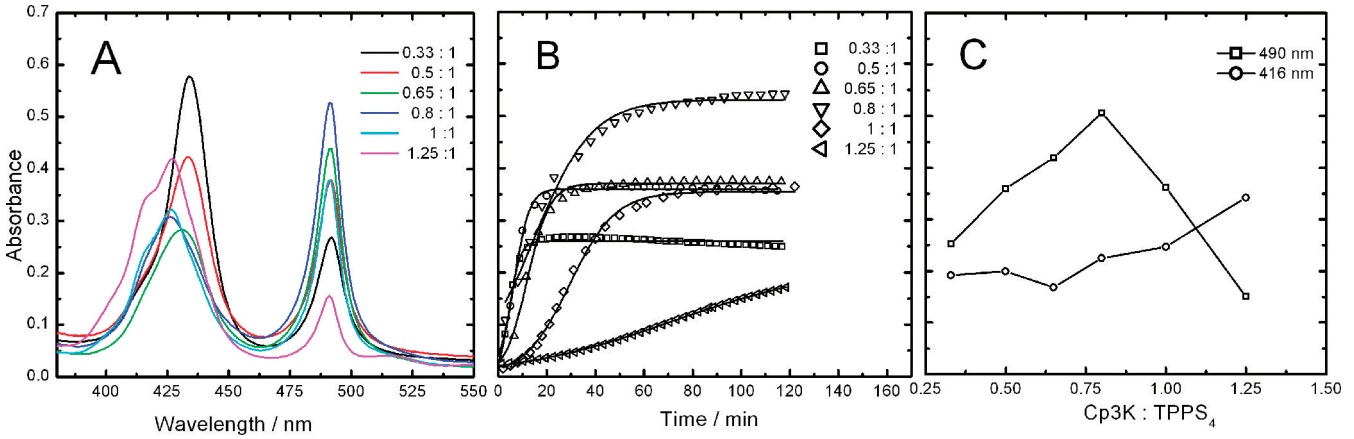

Figure 4. Absorbance of 20 μM $TPPS_4$ upon increasing Cp3K concentration. (A) Spectra were collected at 25 °C after equilibration for about two hours (in 20 mM formic acid, pH 3.5). (B) Kinetics of $TPPS_4$ J-aggregate assembly as a function of Cp3K concentration, monitored at 490 nm. The data are shown fit to a kinetic function to extract time constant and lag parameters; the parameter values are reported in Table 2. (C) Absorbances of 490 and 416 nm bands were plotted as a function of the Cp3K–$TPPS_4$ ratio.

bound in a helical conformation, thus, confirming our initial hypothesis.

We were intrigued by the kinetic aspect to J-aggregate formation seen in both the CD and UV–visible spectroscopy data (Figure 3) and chose to explore this more deeply to give us mechanistic insight into the self-assembly of this biomaterial. As noted above, we observed a slow increase in the magnitude of the 490 nm band with a concomitant decrease in the Soret band at 434 nm (Figure 3A). However, we also noted evidence of bands at 416/424 nm, as shown more clearly in Figure S2. The data in Figure 3A suggest that, at early time points, the 416/424 complex is formed, and at a later time, there is a conversion from this initial complex to a presumably more thermodynamically stable J-aggregate complex. Whether the conversion between the two complexes requires monomeric $TPPS_4$ as an intermediate will be discussed below. In short, the 416/424 complex might act as an obligatory intermediate in J-aggregate assembly, or more likely, as we argue below, this complex represents a separate but parallel path in the self-assembly of $TPPS_4$ monomers.

Interestingly, the kinetics of J-aggregate formation depend strongly on peptide concentration (Figure 4), with the rate of J-aggregate formation decreasing as the peptide concentration increases. At a 1:1 ratio (the standard condition for the experiments described above), a significant lag is evident in the emergence of the 490 nm band, and any further increase in peptide concentration beyond the 1:1 ratio results in an increased inhibitory effect on the self-assembly kinetics (Figure 4B). Below the 1:1 ratio, the lag appears to decrease significantly. These observations are mirrored by the kinetics of the decrease in the 416/424 nm absorbance bands.

It is informative to look at the consequence of varying the peptide concentration on the resultant spectra (Figure 4A). We observe a weak J-aggregate band at subsaturating concen-

dx.doi.org/10.1021/bm201354m | Biomacromolecules 2011, 12, 4196–4203

trations of peptide due simply to the presence of a significant fraction of unbound $TPPS_4$. This 490 nm band increases in intensity as the peptide concentration increases, up until excess peptide begins to induce its inhibitory kinetic effect, at which point a decrease in this band becomes apparent. This effect can be more clearly depicted by plotting the absorbance of the 490 nm band as a function of the ratio of peptide and porphyrin (Figure 4C). The drop off in absorbance for the 490 nm band is largely coincident with an increase in absorbance of the 416 nm band, consistent with the emergence of a new 416/424 complex at higher peptide concentrations, and confined to early time points.

To treat these kinetic data quantitatively, we applied a kinetic function (see Experimental Section) to extract both the lag and time constant parameters (Table 2) and noted a general

Table 2. Parameters from Fit to UV-Visible Kinetic Data

Cp3K/$TPPS_4$ ratio	lag ± std error (min)	time constant ± std error (min)	A_{max}
0.33	4.58 ± 0.14	2.16 ± 0.13	0.26
0.50	6.46 ± 0.11	3.11 ± 0.10	0.36
0.65	11.87 ± 0.26	4.61 ± 0.24	0.37
0.80	14.76 ± 0.66	11.89 ± 0.75	0.53
1.00	29.38 ± 0.34	9.36 ± 0.28	0.35
1.25	71.61 ± 0.67	32.62 ± 0.32	0.21

increase in their values (reflecting a decrease in J-aggregation rate) with increasing peptide concentration. It is unlikely that this kinetic effect is simply due to electrostatic screening of the sulfonates; rather, such screening effects increase the rate of J-aggregation, as shown in work by others.[15]

The unusual peptide concentration dependence of the rate of J-aggregate assembly suggests the possibility of a competing complex, when taken together with the reciprocal relationship in absorbances for the J-aggregate and 416/424 complex. Additional evidence for such a second complex comes from the observation that the magnitude of the absorbance at 434 nm (representing the $TPPS_4$ monomer pool) is greatly reduced immediately upon mixing with high peptide concentrations and matches the rapid acquisition of the 416/424 nm bands (Figure S3). We had also observed the rapidity of self-assembly of the 416/424 complex when measured at neutral pH.[9] The spectra at neutral pH closely matches our resultant spectra collected at pH 3.5 at the highest peptide concentrations and at early time points (under conditions when the amount of J-aggregation is limited; Figure 5). Furthermore, the Q-bands (inset, Figure 5) also show identical intensities and wavelength shifts for the peptide-bound form, irrespective of pH. As a side note, upon peptide binding, the wavelength positions of the Q_x bands (at 594 and 645 nm) are at the same positions as those expected for the acidic form of $TPPS_4$ alone, whereas the Q_y bands (at 515 and 552 nm) reside at positions seen for the neutral pH form of $TPPS_4$. This hybrid distribution of the Q-bands is unusual and must reflect strong electron-withdrawing effects of the peptide that dominate the effects of pH on the electronic state of the porphyrin.

It is worth pointing out that a lag in J-aggregate assembly has been observed in earlier work from another laboratory and was interpreted as involving an autocatalytic pathway in which a high-energy aggregation nucleus is required for assembly to proceed.[68] However, we do not believe that this is the operating principle in our studies because this lag behavior is dependent

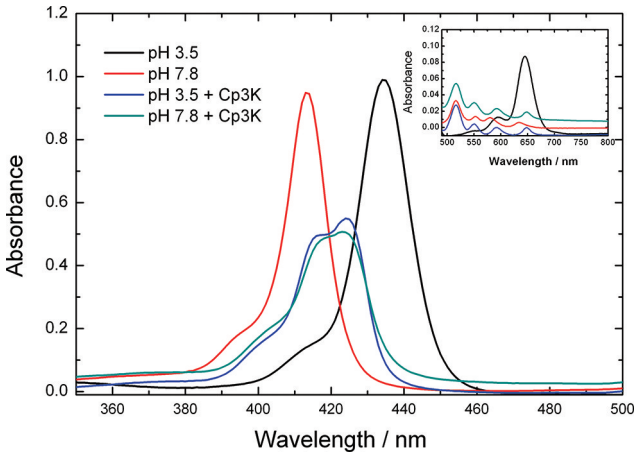

Figure 5. Absorbance spectra of 20 μM $TPPS_4$ in the absence and presence of 40 μM Cp3K in 10 mM Tris-HCl, pH 7.8 or formic acid, pH 3.5, collected at 25 °C. Inset: $TPPS_4$ Q-bands.

on the addition of Cp3K at high concentrations and appears to correlate instead with the acquisition of a 416/424 complex, as described above. If we assume that the rapid acquisition of significant amounts of the 416/424 complex is what results in decreasing the rate of assembly of porphyrin J-aggregate, then it is hard to imagine that the 416/424 complex is a requisite intermediate in J-aggregation, because increasing such an intermediate complex should instead act to increase the rate of this second reaction by mass action. Instead, we argue that the 416/424 complex lies along a separate assembly pathway, and the decrease in the kinetics of J-aggregation is caused by the required disassembly of the 416/424 complex to provide the monomer pool necessary to form J-aggregates.

Insight into the stoichiometry of the peptide and porphyrin complex in the polymer represented by the 490 nm band can be gained by looking at the disappearance of the 434 band as a function of the Cp3K–$TPPS_4$ ratio at times when the complexes have reached equilibrium (Figure S4). Based on two different analytical approaches, as described in the legend for Figure S4, the stoichiometry appears to be in the range of 0.62–0.71, which is close to what would be expected for a 2:3 peptide/porphyrin complex. These experiments allow us to offer the following conclusions: the 1:1 complex (416/424 nm signature) forms rapidly at higher peptide to porphyrin ratios but is perhaps less thermodynamically stable than the 2:3 complex (490 nm signature), whereas the 2:3 complex forms preferentially when the peptide concentration is substoichiometric relative to the porphyrin concentration due to simple principles of mass action.

Based on our results published earlier,[9,10] and the new spectroscopic results presented here, we propose two working models that represent our mesoscale structures (Figure 6). We have strong evidence for the 1:1 Cp3K–$TPPS_4$ structure from our previous work, suggesting that three sulfonates from $TPPS_4$ are engaging the three lysines of a single CP3K peptide (Figure 6A). After peptide-induced polymerization of the Cp3K–$TPPS_4$ complex, we proposed weak excitonic coupling between adjacent $TPPS_4$ molecules based on fluorescence experiments. In this neutral pH model, it is possible that the 424 nm band represents the impact of the binding of the peptide on $TPPS_4$ absorbance. We propose that the second, 416 nm, band results from weak interactions between porphyrins on separate polymers that might be akin to H-aggregation, as suggested

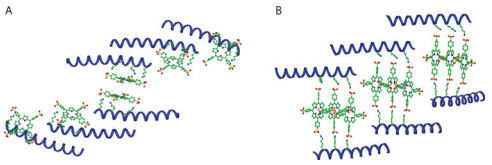

Figure 6. Models illustrating putative structures of (A) 416/424 complex (superstoichiometric ratio of peptide and porphyrin) vs (B) 490 J-aggregate complex (substoichiometric ratio of peptide and porphyrin). (A) The model is adapted from Kokona et al.,[9] showing two polymers forming a fibril through putative $TPPS_4$ H-interactions between individual polymers. (B) The model highlights J-aggregation between porphyrins, in which the helical peptide acts as a scaffold to neutralize the charged sulfonates that are not engaged in porphyrin–porphyrin ionic interactions.

in Figure 6. Such blue-shifting in the spectral features is a hallmark of $TPPS_4$ H-aggregates.[15,16,69]

Based principally on the pH 3.5 data presented here, we propose a second model that represents J-aggregate stacking of $TPPS_4$, in which each lysine on Cp3K interacts with a separate porphyrin. Because two sulfonates per $TPPS_4$ are available for such ionic interaction, it is possible that three porphyrins forming J-aggregate type interactions can be coordinated with two peptides, giving the 2:3 Cp3K–$TPPS_4$ ratio that we suggest (Figure 6B). These models are attractive because the kinetics of conversion from the 416/424 nm complex to the 490 nm J-aggregate are consistent with the proposed stoichiometries and J-aggregate assembly kinetics. Furthermore, the binding of Cp3K to porphyrin in the 1:1 stoichiometry has been well characterized and is only moderately tight, in the low micromolar range.[10] The overall strengths of the peptide–peptide and peptide–porphyrin interactions suggest a ready conversion to the 2:3 complex, which we believe to be more stable, because it involves strong porphyrin–porphyrin π–π and σ–π interactions[70] in addition to the ionic peptide–porphyrin interactions and peptide-specific hydrophobic driving force. Thus, the working models presented in Figure 6 effectively represent the data that we present in this work.

The model with the 2:3 stoichiometry, involving close interaction between neighboring porphyrins, also promises stronger excitonic coupling than that which is suggested in our original model. To test this, we looked at the fluorescence of this complex (Figure 7). Upon excitation at an absorption wavelength where both free porphyrin and peptide-bound porphyrin are equal in intensity (453 nm), we see a slightly quenched fluorescence signal at time zero postmixing. Interestingly, we note a slow decrease in the fluorescence with time, similar to what we observed in our visible spectra, indicating that, as J-aggregation is induced, further quenching results. This is an important result because such quenching suggests strong excitonic coupling between porphyrins with prospects for significant photoelectronic conductivity. This result contrasts with that we had observed in our previous work at neutral pH, in which fluorescence enhancement was seen instead upon self-assembly.[9]

Finally, we probed the mesoscale morphology of the two species using AFM (Figure 8). When the porphyrin is in excess over peptide (conditions that result in J-aggregation), well-defined filaments are seen (Figure 8A). The structures are about 27 nm in height (Figure 8C) and varying in length from 2 to 25 μm. The observed height represents a fair degree of bundling of J-aggregate structures since J-aggregate nanorods

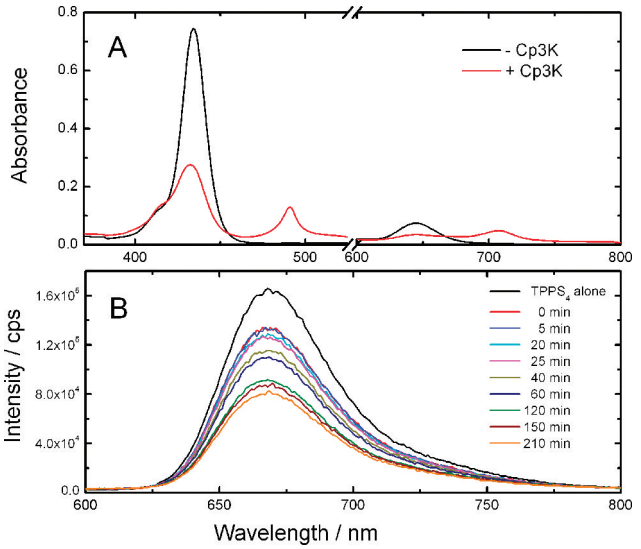

Figure 7. Absorbance and fluorescence spectra of $TPPS_4$ in the presence and absence of Cp3K. (A) Absorbance spectra of $TPPS_4$ alone and a mixture of 20 μM $TPPS_4$ with 6.67 μM Cp3K, in 20 mM formic acid, pH 3.5. (B) Fluorescence spectra of $TPPS_4$ alone and a mixture of 20 μM $TPPS_4$ with 6.67 μM Cp3K $TPPS_4$ collected over time under the same sample conditions as in (A).

made up of $TPPS_4$ alone are typically in the 4–5 nm range in height and 50 nm in length.[27] However, when the peptide is in excess, amorphous aggregates are seen (Figure 8B) that are similar to structures that we had observed previously.[9] The filamentous behavior observed by AFM, when combined with our evidence for strong excitonic coupling, provides promising characteristics for future photoelectronic conductivity measurements.

CONCLUSIONS

We have shown that we can modulate the assembly of an electronically active material in a pH-dependent manner by designing specific interactions between a coiled-coil peptide scaffold and an anionic porphyrin. Using UV–visible spectroscopy, we have clearly illustrated how the anionic porphyrin, $TPPS_4$, is able to form J-aggregate structures at intermediate acidic conditions upon noncovalent binding of our positively charged coiled-coil forming peptide, Cp3K. Using circular dichroism spectropolarimetry, we have verified that self-assembly into large polymers depends upon the helical nature of our peptide, supporting the importance of coiled-coil interactions in regulating self-assembly processes. Most importantly, fluorescence experiments suggest a significant degree of quenching upon self-assembly, suggesting great promise for a photoelectronically active conductive material.

The involvement of a peptide whose structure is well-established means that it is now possible to modulate the assembly with greater precision. For example, given the nature of the peptide–peptide interactions, the polymerization is reversible through such mechanisms as simple as dilution or by temperature-induced unfolding. Other "switches" can be added; for example, in a separate effort, we have worked on incorporating an azobenzene group[71] to create light-sensitive activation of the peptide polymerization process (BK, unpublished data). Interestingly, depending on the ratio of peptide to porphyrin, we could induce different types of polymers usuing precise kinetic control. One polymer is similar

dx.doi.org/10.1021/bm201354m | Biomacromolecules 2011, 12, 4196–4203

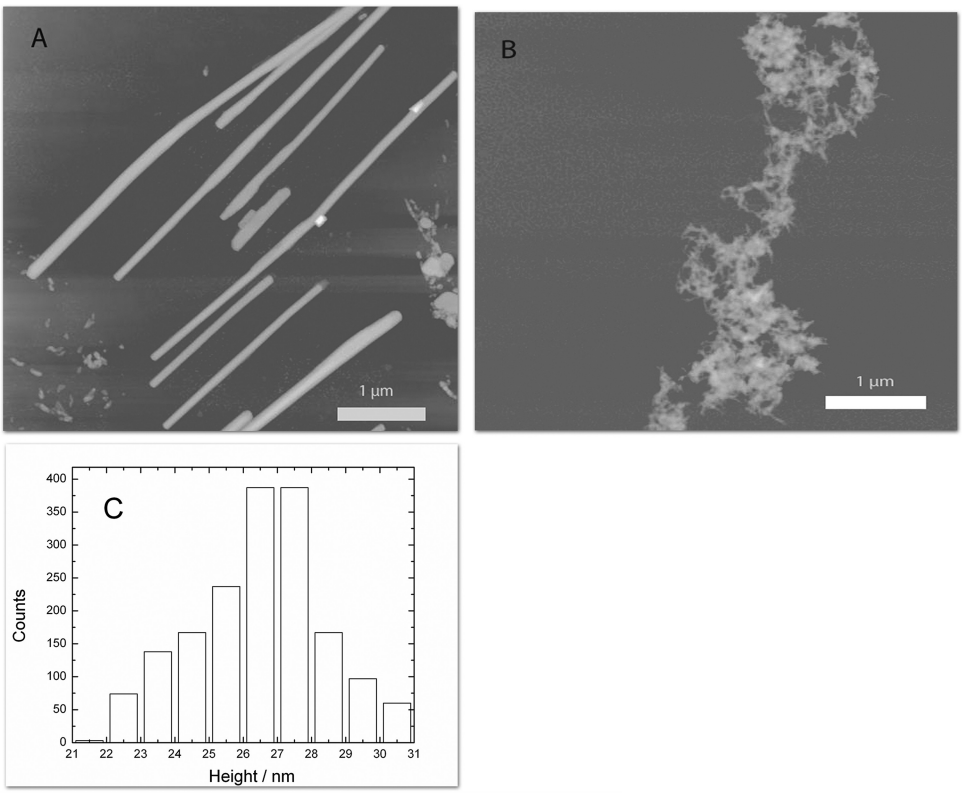

Figure 8. AFM topography of $TPPS_4$/Cp3K polymers. (A) Samples were prepared at a 1:2 ratio of Cp3K/$TPPS_4$ in 20 mM formic acid, pH 3.5, and deposited on freshly cleaved mica. (B) Samples were prepared at a 2:1 ratio of Cp3K/$TPPS_4$ in 20 mM formic acid, pH 3.5. (C) Histogram representing a height analysis of the polymers shown in (A).

to what we had observed at neutral pH,[9] and the second polymer represents a novel structure unprecedented in the literature, involving J-aggregation associated with a coiled-coil scaffold. These results demonstrate the ability to modulate different assembly pathways through simple biochemical approaches. AFM imaging of this new polymer shows a much more homogeneous fibrillar structure than what we had previously observed and shows great promise for future photoconductivity studies, which are currently underway. The average diameter of pure $TPPS_4$ nanorods is 3.8 nm, however, aging of the samples can result in bundles with heights in the range of 15−50 nm and are quite heterogeneous in nature.[29] The heights of our fibrils are uniformly about 27 nm, suggesting some degree of bundling. Therefore, inclusion of the peptide in this material appears to modulate lateral assembly processes. It will be interesting to compare the effects of the peptide on the conduction properties of these fibrils to those published previously for $TPPS_4$ nanorods.[21,23] The homogeneity and persistence length of our fibrils should offer the engineering characteristics necessary for robust deposition onto a variety of surfaces, with the long-term goal of creating precisely deposited materials to create novel circuits at the nanoscale.[5]

■ ASSOCIATED CONTENT

Supporting Information

pH dependence of $TPPS_4$ absorbance in the absence and presence of Cp3K; absorbance spectra of $TPPS_4$ in the absence and presence of Cp3K at a 1:1 ratio; kinetics of disappearance of $TPPS_4$ monomer as a function of Cp3K concentration; and absorbance of diacid form of $TPPS_4$ as a function of Cp3K−$TPPS_4$ ratio. This material is available free of charge via the Internet at http://pubs.acs.org.

■ AUTHOR INFORMATION

Corresponding Author

*Tel.: (610) 896-4205. Fax: (610) 896-4963. E-mail: rfairman@haverford.edu.

■ ACKNOWLEDGMENTS

This research was supported by grants from NSF (CHE-0616615 and MCB-0516025 to R.F.), and grants to Haverford College from the Arnold and Mabel Beckman Foundation and the HHMI Undergraduate Science Education Program to support undergraduate research. We thank Elizabeth Welch for technical assistance and Andrew McNeal for help in preparing the molecular graphics images. We also thank Cristina Fuller for help with editing the manuscript.

■ REFERENCES

(1) Kyle, S.; Aggeli, A.; Ingham, E.; McPherson, M. J. *Trends Biotechnol.* **2009**, *27*, 423−433.
(2) Chen, C. L.; Rosi, N. L. *Angew. Chem., Int. Ed.* **2010**, *49*, 1924−1942.
(3) McAllister, K. A.; Zou, H.; Cochran, F. V.; Bender, G. M.; Senes, A.; Fry, H. C.; Nanda, V.; Keenan, P. A.; Lear, J. D.; Saven, J. G.; Therien, M. J.; Blasie, J. K.; DeGrado, W. F. *J. Am. Chem. Soc.* **2008**, *130*, 11921−11927.
(4) Fairman, R.; Akerfeldt, K. S. *Curr. Opin. Struct. Biol.* **2005**, *15*, 453−463.
(5) Pepe-Mooney, B. J.; Fairman, R. *Curr. Opin. Struct. Biol.* **2009**, *19*, 483−494.

(6) Chockalingam, K.; Blenner, M.; Banta, S. *Protein Eng., Des. Sel.* **2007**, *20*, 155−161.
(7) Krishna, O. D.; Kiick, K. L. *Biopolymers* **2010**, *94*, 32−48.
(8) Dublin, S.; Zimenkov, Y.; Conticello, V. P. *Biochem. Soc. Trans.* **2009**, *37*, 653−659.
(9) Kokona, B.; Kim, A. M.; Roden, R. C.; Daniels, J. P.; Pepe-Mooney, B. J.; Kovaric, B. C.; de Paula, J. C.; Johnson, K. A.; Fairman, R. *Biomacromolecules* **2009**, *10*, 1454−1459.
(10) Kovaric, B. C.; Kokona, B.; Schwab, A. D.; Twomey, M. A.; de Paula, J. C.; Fairman, R. *J. Am. Chem. Soc.* **2006**, *128*, 4166−4167.
(11) Wagner, D. E.; Phillips, C. L.; Ali, W. M.; Nybakken, G. E.; Crawford, E. D.; Schwab, A. D.; Smith, W. F.; Fairman, R. *Proc. Natl. Acad. Sci. U.S.A.* **2005**, *102*, 12656−12661.
(12) Apostolovic, B.; Danial, M.; Klok, H. -A. *Chem. Soc. Rev.* **2010**, *39*, 3541−3575.
(13) Woolfson, D. N. *Biopolymers* **2010**, *94*, 118−127.
(14) Woolfson, D. N.; Mahmoud, Z. N. *Chem. Soc. Rev.* **2010**, *39*, 3464−3479.
(15) Aggarwal, L. P. F.; Borissevitch, I. E. *Spectrochim. Acta, Part A* **2006**, *63*, 227−233.
(16) Egawa, Y.; Hayashida, R.; Anzai, J. I. *Langmuir* **2007**, *23*, 13146−13150.
(17) Augulis, R.; Snitka, V.; Rotomskis, R. *Solid State Phenom.* **2004**, *97*−*98*, 191−194.
(18) Augulis, R.; Tamuliene, J.; Tamulis, A.; Rotomskis, R. *Solid State Phenom.* **2004**, *97*−*98*, 225−228.
(19) Augulis, R.; Valiokas, R.; Liedberg, B.; Rotomskis, R. *Solid State Phenom.* **2004**, *97*−*98*, 195−200.
(20) Ohno, O.; Kaizu, Y.; Kobayashi, H. *J. Chem. Phys.* **1993**, *99*, 4128−4139.
(21) Schwab, A. D.; Smith, D. E.; Bond-Watts, B.; Johnston, D. E.; Hone, J.; Johnson, A. T.; de Paula, J. C.; Smith, W. F. *Nano Lett.* **2004**, *4*, 1261−1265.
(22) Crusats, J.; El-Hachemi, Z.; Escudero, C.; Ribo, J. M. *J. Porphyrins Phthalocyanines* **2009**, *13*, 461−470.
(23) Yeats, A. L.; Schwab, A. D.; Massare, B.; Johnston, D. E.; Johnson, A. T.; de Paula, J. C.; Smith, W. F. *J. Phys. Chem. C* **2008**, *112*, 2170−2176.
(24) Wu, J. J.; Li, N.; Li, K. A.; Liu, F. *J. Phys. Chem. B* **2008**, *112*, 8134−8138.
(25) Rahimi, R.; Jeddi, M.; Mohammad, S.; Ravanfar, R. *Asian J. Chem.* **2009**, *21*, 3988−3994.
(26) Arai, Y.; Segawa, H. *Chem. Commun. (Cambridge, U. K.)* **2010**, *46*, 4279−4281.
(27) Hosomizu, K.; Oodoi, M.; Umeyama, T.; Matano, Y.; Yoshida, K.; Isoda, S.; Isosomppi, M.; Tkachenko, N. V.; Lemmetyinen, H.; Imahori, H. *J. Phys. Chem. B* **2008**, *112*, 16517−16524.
(28) Rotomskis, R.; Augulis, R.; Snitka, V.; Valiokas, R.; Liedberg, B. *J. Phys. Chem. B* **2004**, *108*, 2833−2838.
(29) Schwab, A. D.; Smith, D. E.; Rich, C. S.; Young, E. R.; Smith, W. F.; de Paula, J. C. *J. Phys. Chem. B* **2003**, *107*, 11339−11345.
(30) Snitka, V.; Rackaitis, M.; Rodaite, R. *Sens. Actuators, B* **2005**, *109*, 159−166.
(31) Fleischer, E. B.; Palmer, J. M.; Srivastava, T. S.; Chatterjee, A. *J. Am. Chem. Soc.* **1971**, *93*, 3162−3167.
(32) Pasternack, R. F.; Centuro, G. C.; Boyd, P.; Hinds, L. D.; Huber, P. R.; Francesc., L; Fasella, P.; Engasser, G.; Gibbs, E. *J. Am. Chem. Soc.* **1972**, *94*, 4511−4517.
(33) Ribo, J. M.; Crusats, J.; Farrera, J. A.; Valero, M. L. *J. Am. Chem. Soc.* **1994**, 681−682.
(34) Synytsya, A.; Synytsya, A.; Blafkova, P.; Ederova, J.; Spevacek, J.; Slepicka, P.; Kral, V.; Volka, K. *Biomacromolecules* **2009**, *10*, 1067−1076.
(35) Synytsya, A.; Synytsya, A.; Blafkova, P.; Volka, K.; Kral, V. *Spectrochim. Acta, Part A* **2007**, *66*, 225−235.
(36) Pasternack, R. F.; Gibbs, E. J. *Met. Ions Biol. Syst.* **1996**, *33*, 367−397.
(37) Gandini, S. C. M.; Yushmanov, V. E.; Perussi, J. R.; Tabak, M.; Borissevitch, I. E. *J. Inorg. Biochem.* **1999**, *73*, 35−40.
(38) Postigo, F.; Mora, M.; De Madariaga, M. A.; Nonell, S.; Sagrista, M. L. *Int. J. Pharm.* **2004**, *278*, 239−254.
(39) Prochazka, M.; Stepanek, J.; Turpin, P. Y. *Chem. Phys. Lipids* **2004**, *132*, 145−156.
(40) Ricchelli, F.; Gobbo, S.; Moreno, G.; Salet, C.; Brancaleon, L.; Mazzini, A. *Eur. J. Biochem.* **1998**, *253*, 760−765.
(41) Andrade, S. M.; Costa, S. M. B. *Biophys. J.* **2002**, *82*, 1607−1619.
(42) Andrade, S. M.; Costa, S. M. B. *J. Fluoresc.* **2002**, *12*, 77−82.
(43) Aoudia, M.; Guliaev, A. B.; Leontis, N. B.; Rodgers, M. A. *Biophys. Chem.* **2000**, *83*, 121−140.
(44) Aoudia, M.; Rodgers, M. A. J. *Langmuir* **2005**, *21*, 10355−10361.
(45) Arai, T.; Inudo, M.; Ishimatsu, T.; Akamatsu, C.; Tokusaki, Y.; Sasaki, T.; Nishino, N. *J. Org. Chem.* **2003**, *68*, 5540−5549.
(46) Arai, T.; Inudo, M.; Ishimatsu, T.; Sasaki, T.; Kato, T.; Nishino, N. *Chem. Lett.* **2001**, 1240−1241.
(47) Dunetz, J. R.; Sandstrom, C.; Young, E. R.; Baker, P.; Van Name, S. A.; Cathopolous, T.; Fairman, R.; de Paula, J. C.; Akerfeldt, K. S. *Org. Lett.* **2005**, *7*, 2559−2561.
(48) Fukushima, Y. *Polym. Bull.* **2001**, *45* (6), 479−485.
(49) Huang, C. Z.; Liu, Y.; Wang, Y. H.; Guo, H. P. *Anal. Biochem.* **2003**, *321*, 236−243.
(50) Kuciauskas, D.; Caputo, G. A. *J. Phys. Chem. B* **2009**, *113*, 14439−14447.
(51) Kuciauskas, D.; Riskis, J.; Caputo, G. A.; Gulbinas, V. *J. Phys. Chem. B* **2010**, *114*, 16029−16035.
(52) Purrello, R.; Bellacchio, E.; Gurrieri, S.; Lauceri, R.; Raudino, A.; Scolaro, L. M.; Santoro, A. M. *J. Phys. Chem. B* **1998**, *102*, 8852−8857.
(53) Solladie, N.; Aubert, N.; Bouatra, S.; Bourgogne, C.; Bregier, F.; Brettar, J.; Gisselbrecht, J. P.; Gross, M.; Rein, R.; Sooambar, C.; Troiani, V.; Walther, M. *J. Porphyrins Phthalocyanines* **2003**, *7*, 270−281.
(54) Takahashi, M.; Ueno, A.; Mihara, H. *Chem.—Eur. J.* **2000**, *6*, 3196−3203.
(55) Takahashi, M.; Ueno, A.; Uda, T.; Mihara, H. *Bioorg. Med. Chem. Lett.* **1998**, *8*, 2023−2026.
(56) Tian, F.; Johnson, E. M.; Zamarripa, M.; Sansone, S.; Brancaleon, L. *Biomacromolecules* **2007**, *8*, 3767−3778.
(57) Urbanova, M.; Setnicka, V.; Kral, V.; Volka, K. *Biopolymers* **2001**, *60* (4), 307−16.
(58) Valanciunaite, J.; Bagdonas, S.; Streckyte, G.; Rotomskis, R. *Photochem. Photobiol. Sci.* **2006**, *5*, 381−388.
(59) Venkatesh, B.; Jayakumar, R.; Pandian, R. P.; Manoharan, P. T. *Biochem. Biophys. Res. Commun.* **1996**, *223*, 390−396.
(60) Zhang, L.; Liu, M. H. *J. Phys. Chem. B* **2009**, *113*, 14015−14020.
(61) Koti, A. S. R.; Periasamy, N. *Chem. Mater.* **2003**, *15*, 369−371.
(62) Koti, A. S. R.; Taneja, J.; Periasamy, N. *Chem. Phys. Lett.* **2003**, *375*, 171−176.
(63) Purrello, R.; Raudino, A.; Scolaro, L. M.; Loisi, A.; Bellacchio, E.; Lauceri, R. *J. Phys. Chem. B* **2000**, *104*, 10900−10908.
(64) Wang, Q. B.; Chen, Y. L.; Ma, P.; Lu, J. T.; Zhang, X. M.; Jiang, J. Z. *J. Mater. Chem.* **2011**, *21*, 8057−8065.
(65) Rosen, H. *Arch. Biochem. Biophys.* **1957**, *67* (1), 10−5.
(66) Zeng, L. X.; He, Y. J.; Dai, Z. F.; Wang, J.; Cao, Q.; Zhang, Y. L. *ChemPhysChem* **2009**, *10*, 954−962.
(67) Arutyunyan, A. M.; Rafikova, E. R.; Drachev, V. A.; Dobrov, E. N. *Biochemistry (Moscow)* **2001**, *66*, 1378−1380.
(68) Pasternack, R. F.; Fleming, C.; Herring, S.; Collings, P. J.; dePaula, J.; DeCastro, G.; Gibbs, E. J. *Biophys. J.* **2000**, *79*, 550−560.
(69) Zhao, L. Z.; Ma, R. J.; Li, J. B.; Li, Y.; An, Y. L.; Shi, L. Q. *Biomacromolecules* **2008**, *9*, 2601−2608.
(70) Hunter, C. A.; Sanders, J. K. M. *J. Am. Chem. Soc.* **1990**, *112*, 5525−5534.
(71) Beharry, A. A.; Woolley, G. A. *Chem. Soc. Rev.* **2011**, *40*, 4422−4437.

SUPPORTING INFORMATION

Characterization of mesoscale coiled-coil peptide-porphyrin complexes.

*Brian J. Pepe-Mooney, Bashkim Kokona, and Robert Fairman**

Department of Biology, Haverford College, 370 Lancaster Ave, Haverford, PA 19041

RECEIVED DATE

TITLE RUNNING HEAD: Peptide-Porphyrin Biomaterials

*Author to whom correspondence should be addressed. Tel.: (610) 896-4205; Fax: (610) 896-4963; email: rfairman@haverford.edu

Figure S1. pH dependence of $TPPS_4$ absorbance in the (A) absence or (B) presence of Cp3K. The porphyrin and peptide concentrations were 20 μM each, prepared in 10 mM each of the sodium salts of phosphate, citrate, and borate and measured at 25°C.

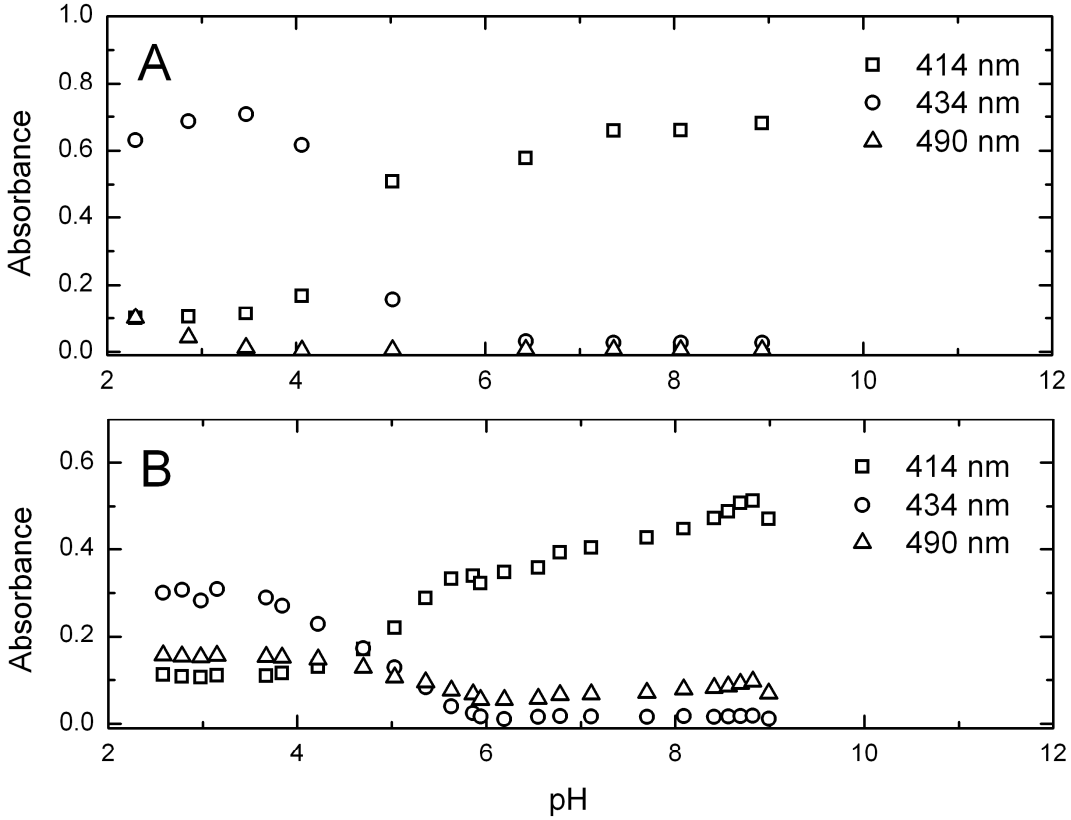

Figure S2. Absorbance spectra of 20 μM $TPPS_4$ in the absence and presence of 20 μM Cp3K in 10 mM Tris-HCl, pH 7.8 or formic acid, pH 3.5 collected at 25°C. Inset: $TPPS_4$ Q-bands.

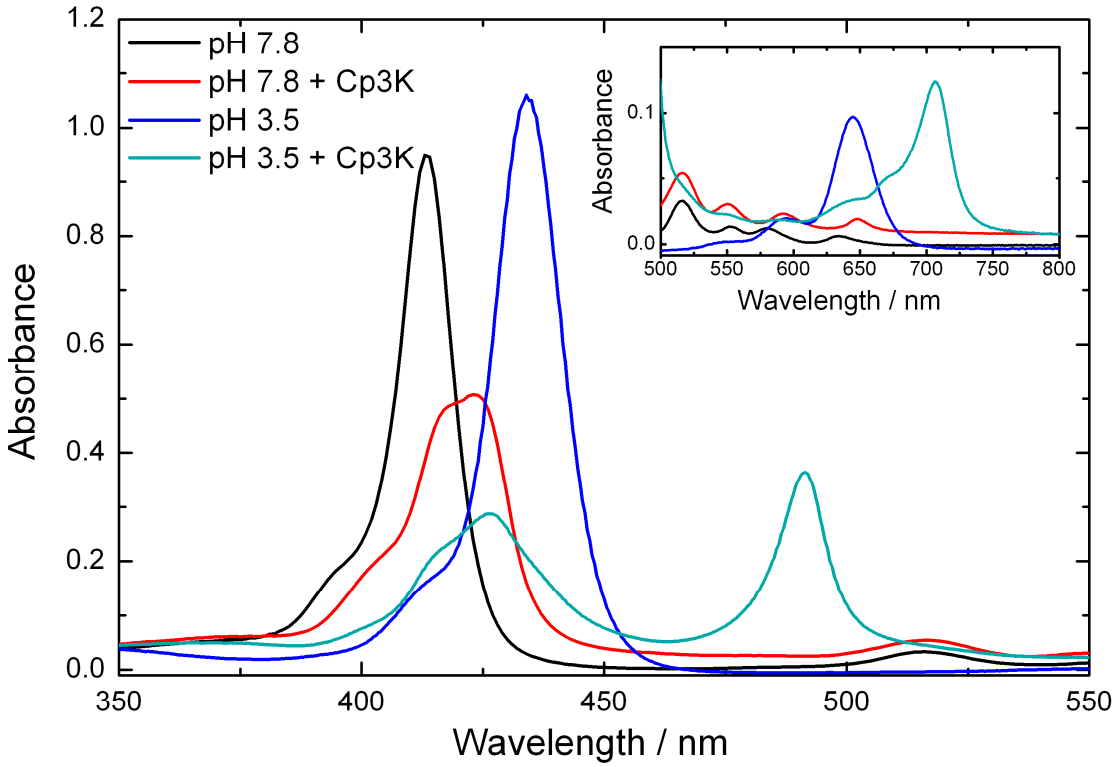

Figure S3. Kinetics of disappearance of $TPPS_4$ monomer as a function of Cp3K concentration, monitored at 434 nm. Conditions are the same as described in Figure 4 and the data are fit to the same equation used to analyze the data in Figure 4B.

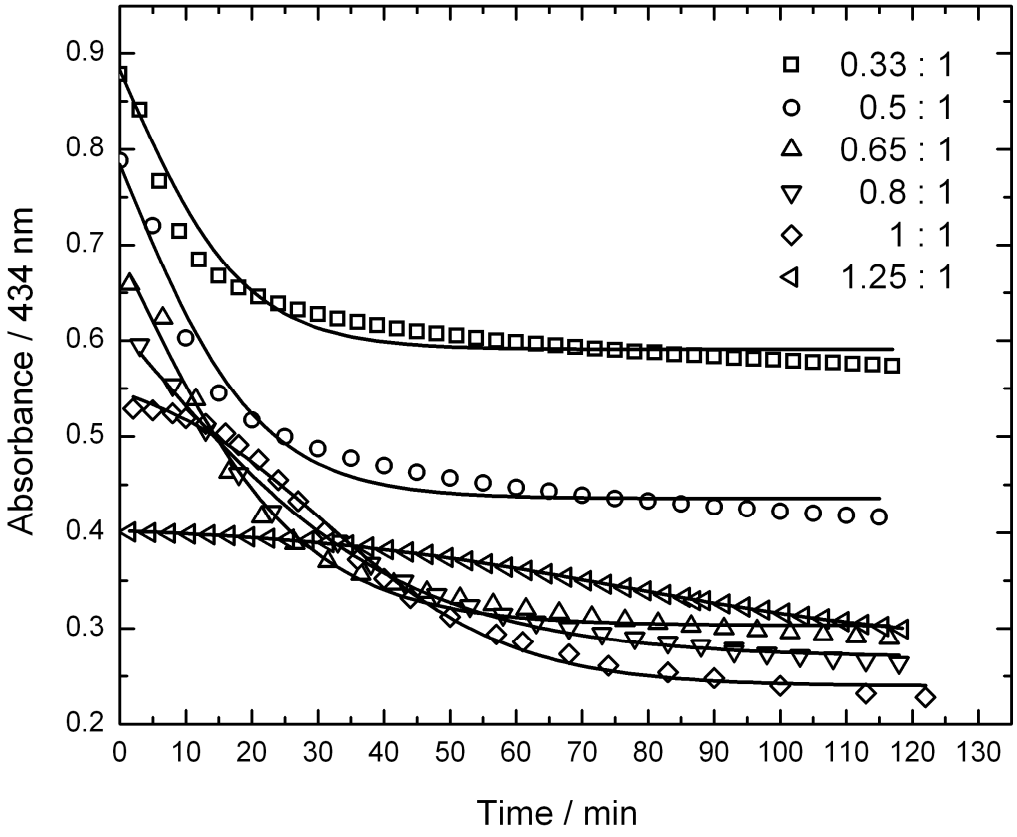

Figure S4. Absorbance of di-acid form of $TPPS_4$ as a function of Cp3K-$TPPS_4$ ratio. The sample was prepared in 20 mM formic acid, pH 3.5 and measured at 25°C. The absorbance of the 434 nm band appears to drop off and plateau between a peptide-porphyrin ratio of 0.5 and 1.0. We took two approaches to define this break in the data more precisely. In the first approach, the first four, and last four, data points were fit with linear functions to highlight a crossover point that is at 0.71 on the x-axis. We also chose to fit this with the Hill equation, which allows for an approximate pseudo-second order dissociation constant to be determined with no requirement for knowing the order of the assembly reaction. We obtained a value for the dissociation constant of 0.31±0.02 (reported as a ratio of peptide to porphyrin). Since this number represents the half-saturation point, it again suggests a 2:3 peptide:porphyrin stoichiometry.